

SPARSE-UP: LEARNABLE SPARSE UPSAMPLING FOR 3D GENERATION WITH HIGH-FIDELITY TEXTURES

Lu Xiao[†], Jiale Zhang[†], Yang Liu, Taicheng Huang^{*}, Xin Tian

JD.com, Beijing, China

ABSTRACT

The creation of high-fidelity 3D assets is often hindered by a ‘pixel-level pain point’: the loss of high-frequency details. Existing methods often trade off one aspect for another: either sacrificing cross-view consistency, resulting in torn or drifting textures, or remaining trapped by the resolution ceiling of explicit voxels, forfeiting fine texture detail. In this work, we propose *Sparse-Up*, a memory-efficient, high-fidelity texture modeling framework that effectively preserves high-frequency details. We use sparse voxels to guide texture reconstruction and ensure multi-view consistency, while leveraging *surface anchoring* and *view-domain partitioning* to break through resolution constraints. *Surface anchoring* employs a learnable upsampling strategy to constrain voxels to the mesh surface, eliminating over 70% of redundant voxels present in traditional voxel upsampling. *View-domain partitioning* introduces an image patch-guided voxel partitioning scheme, supervising and back-propagating gradients only on visible local patches. Through these two strategies, we can significantly reduce memory consumption during high-resolution voxel training without sacrificing geometric consistency, while preserving high-frequency details in textures.

Index Terms— 3D Generation, Texture Synthesis, 3D Modeling

1. INTRODUCTION

3D assets are widely used in the fields of games, films, and e-commerce. In recent years, generative artificial intelligence has achieved remarkable progress in areas such as text[1, 2], images[3, 4], videos[5, 6], and 3D content[7, 8, 9, 10, 11]. Due to the inherent complexity of 3D geometric representation, the generation of 3D content is even more challenging.

Current 3D generation models primarily follow two architectures: two-stage methods compress 3D shapes into latent token sequences for geometry and use multi-view diffusion for texture, but lack explicit geometric constraints, leading to misaligned and blurry textures. Sparse voxel-based methods encode local features via active voxels but face a trade-off:

low resolution misses high-frequency details, while high resolution demands prohibitive memory, limiting detail quality.

Building on the sparse voxel generation framework[10], we seek to break voxel resolution limits and achieve high-fidelity texture modeling. We note that traditional voxel-upsampling algorithms usually start from original voxel vertices and generate eight new ones, but this creates many off-surface points, leading to significant redundancy in voxel representation. By statistically analyzing the training data, we find that 70% of these points are off-surface; such redundancies become the main computational and memory bottleneck in high-resolution training, severely limiting further increases in voxel resolution.

To address this issue, we propose a learnable upsampling scheme called *surface anchoring*. By creating a learnable mapping between redundant upsampled points and true on-surface locations, and designing a network architecture symmetric to the Texture-VAE decoder for end-to-end learning, we effectively eliminate redundant points and boost the efficiency and fidelity of voxel representation.

Nevertheless, high resolutions cause voxel grid points to explode and 3D Gaussians from the Texture-VAE decoder to grow accordingly, keeping GPU memory consumption during rendering high. To further reduce computational overhead, we propose a *view-domain partitioning* strategy: using image patches as units, it culls voxels so only those within the current patch participate in rendering and back-propagation. This approach, leveraging localized rendering and gradient updates, significantly lowers memory usage.

In summary, our main contributions are:

- We propose a *surface anchoring* scheme that learns a mapping from redundant upsampled points to true surface points, eliminating redundancy and enhancing voxel efficiency.
- We introduce a *view-domain partitioning* strategy that performs localized rendering and reconstruction, significantly lowering memory consumption during rendering.
- Experiments demonstrate that our approach has attained state-of-the-art performance in the field of texture reconstruction.

[†]Equal contribution . ^{*}Corresponding author: huangtaicheng.1@jd.com

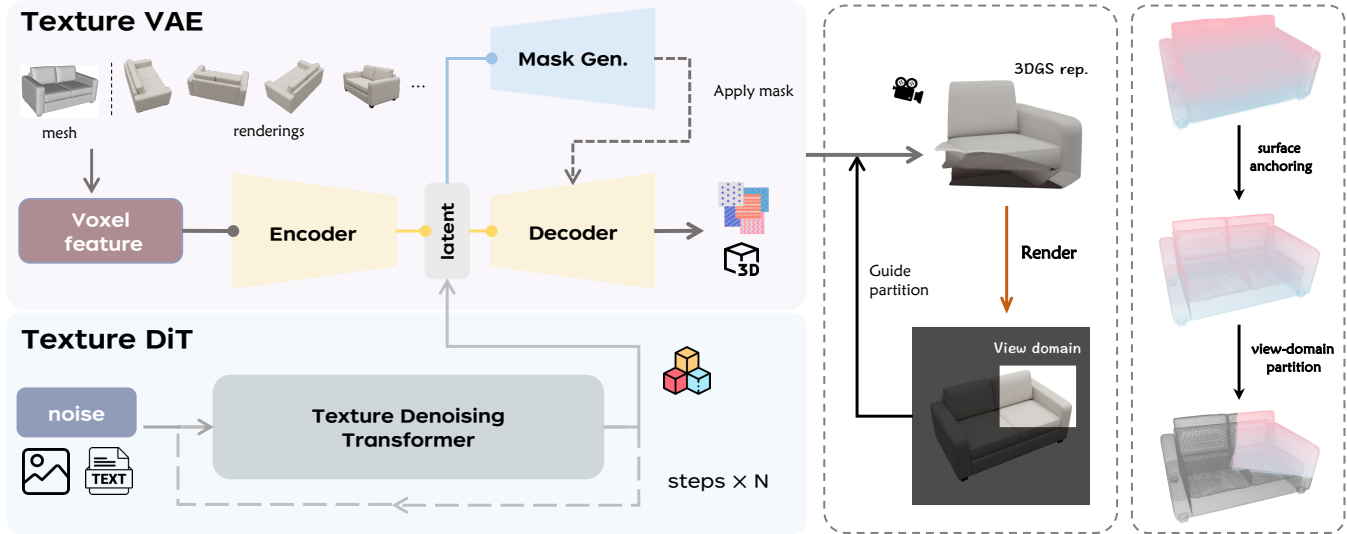


Fig. 1: Overall workflow of the Sparse-Up 3D generation architecture. The workflow modules include Texture-VAE, Mask Generator and Texture-DiT. The right side illustrates the process of removing redundant points to achieve surface anchoring using a MASK generator, as well as local rendering and supervision performed via view-domain partitioning.

2. METHODOLOGY

We introduce Sparse-Up, an end-to-end framework that supports high-resolution and high-fidelity texture modeling, with the overall pipeline illustrated in fig.1. The framework takes sparse voxels embedded with texture features as input and, after a VAE encoder-decoder pass, directly outputs an explicit 3D Gaussian representation (3DGS). This explicit geometry inherently guarantees multi-view consistency. To break the resolution bottleneck, we propose two complementary schemes: *surface anchoring* and *view-domain partitioning*. Section 2.1 presents the learnable surface-anchoring upsampling strategy that accurately maps redundant voxels onto the object surface, while Section 2.2 details the view-domain partitioning mechanism, which performs localized rendering and gradient back-propagation on a per-patch basis to reduce memory consumption.

2.1. Surface-Anchoring Upsampling

To achieve high-resolution reconstruction, we integrate two upsampling modules into the decoder architecture. Traditional upsampling often produces numerous off-surface and redundant points, degrading reconstructed surface quality and causing high memory consumption. To tackle these issues, we introduce an advanced transformer-based Mask Generator to guide redundancy elimination.

Specifically, this component explicitly predicts a mapping mask to transform redundant points into their on-surface counterparts in each upsampling module. This mapping then guides the 3DGS decoder for precise upsampling—removing redundancy while preserving fine surface detail integrity (as shown in fig.2). Thus, our method boosts reconstructed sur-

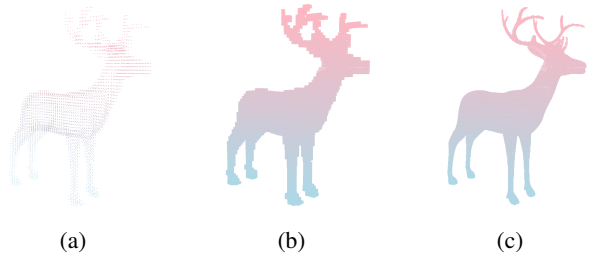


Fig. 2: Comparison of voxel visualizations. (a) Low-resolution original data; (b) Traditional upsampling result (with redundancy); (c) High-resolution data after redundancy removal via generated mask, with approximately 70% of points reduced from (b). It can be observed that high-resolution data contains much richer information than low-resolution data, and the generated mask has effectively eliminated a large number of redundant voxels.

face spatial resolution, retains intricate textures and geometric features critical for high-fidelity 3D models, and reduces memory consumption by eliminating nearly 70% of voxels from traditional voxel upsampling, enabling higher-resolution training.

To explicitly supervise the mask generator, we create ground-truth (GT) masks of different resolutions for 3D models in our dataset. Here, we illustrate the process using a 128-resolution mask as an example. First, each model is voxelized at 64 and 128 resolutions to get surface voxel sets V_{64} and V_{128} . Next, V_{64} undergo a traditional upsampling process to produce \hat{V}_{128} — a 128-resolution voxel set with redundancies, which fully contains V_{128} . Finally, by performing an intersection operation on the voxel coordinates of V_{128} and \hat{V}_{128} , we can derive the GT mask M_{128} that maps \hat{V}_{128} to

V_{128} , as illustrated by the following equation:

$$M_{128}(v) = \begin{cases} 1, & \text{if } v \in V_{128} \\ 0, & \text{otherwise} \end{cases}, \quad \forall v \in \hat{V}_{128}, \quad (1)$$

Note that M_{128} has the same shape as \hat{V}_{128} . Through this process, we generate multi-resolution GT masks for each 3D model to supervise the mask generator. However, the voxel arrangement in \hat{M}_{128} generated by the mask generator via sparse convolution may differ from M_{128} . To ensure precise supervision, we apply a hash mapping from M_{128} to \hat{M}_{128} to align their order for accurate supervision.

This approach enables precise supervision of the mask generator; by leveraging multi-resolution GT masks, the generator is better able to predict masks that remove redundancy while preserving key surface details.

2.2. View-domain Partitioning

To curb the rendering memory footprint while preserving high rendering quality, we propose a novel *view-domain partitioning* strategy. It optimizes computational efficiency and memory usage via localized rendering and updates, with the core idea of splitting the rendering process into smaller, manageable segments—this reduces overall memory load and enables more scalable, efficient training.

Tile-Based Partitioning Strategy. The first step is partitioning the valid image region into uniformly sized, overlapping tiles. Tile overlap is crucial—it avoids boundary discontinuities and artifacts, enabling smooth transitions and high-quality rendering across the entire image region.

During training, tiles are randomly sampled from the partitioned image region, introducing stochasticity that reduces overfitting and improves generalization. Each selected tile then undergoes culling to remove voxels outside its camera frustum, which minimizes memory usage by retaining only relevant voxels for rendering.

Localized Rendering and Updates. The remaining voxels in the selected tile generate 3D Gaussians for localized rendering of the corresponding image patch. Losses are computed and gradients back-propagated only within this patch. Focusing on one patch at a time cuts computational load and memory needs vs. rendering the whole image at once, enabling high-quality rendering with practical memory usage.

2.3. Loss Function

We use the binary cross-entropy loss to supervise the mask generated by the Mask Generator for redundancy removal:

$$L_{mask} = BCE(M, \hat{M}), \quad (2)$$

We train the Texture-VAE in an end-to-end manner, with the objective function as follows[7, 10]:

$$L = \lambda_1 \mathcal{L}_1 + \lambda_2 \mathcal{L}_{SSIM} + \lambda_3 \mathcal{L}_{LPIPS} + \lambda_4 \mathcal{L}_{KL} + \lambda_5 \mathcal{L}_{reg}, \quad (3)$$

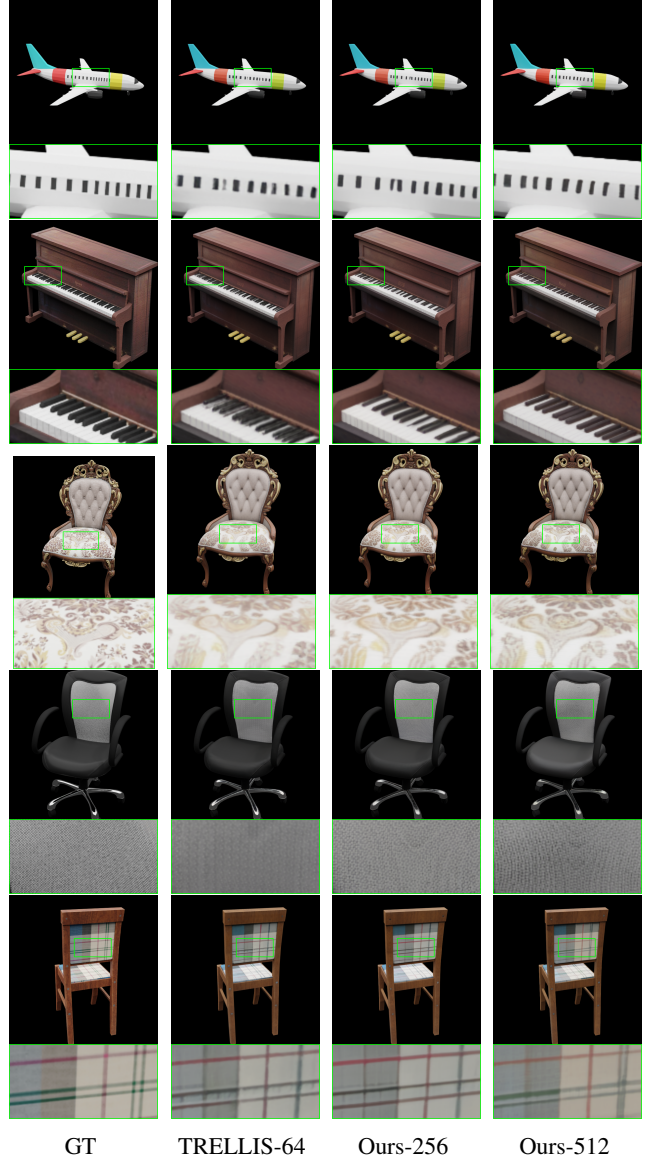


Fig. 3: Qualitative comparison of Texture VAE reconstruction quality between our method with different resolution.

We calculate the L1, D-SSIM, and LPIPS losses between the ground truth (GT) and the 3DGS rendered images output by the Texture-VAE. \mathcal{L}_{KL} is the KL divergence between the learned latent distribution and a standard normal prior, regularizing the latent space. \mathcal{L}_{reg} is a regularization term for the opacity and scale properties of the output 3DGS, which encourages small and opaque Gaussians.

3. EXPERIMENTS

3.1. Experiment Settings

Datasets. We selected a total of 120k high-quality data samples from three datasets, namely Objaverse (XL)[12], ABO[13], and 3D-FUTURE[14], for training the Texture

Table 1: Quantitative comparison of Texture VAE reconstruction quality between our method with different resolution and TRELLIS.

	LPIPS ↓	PSNR ↑	SSIM ↑
TRELLIS-64	0.0219	34.26	0.984
Ours-256	0.0195	34.49	0.984
Ours-512	0.0187	34.97	0.985

Table 2: Quantitative generation results on Toys4k.

	FID ↓	KID ↓
TRELLIS	83.496	5.760×10^{-4}
hunyuan3D 2.1	74.219	4.988×10^{-4}
Step1X-3D	99.620	28.36×10^{-4}
Ours	67.766	3.647×10^{-4}

Variational Autoencoder (VAE) and Latent Space Flow models. Specifically, for the Objaverse (XL)[12] dataset, we used the intersection of the filtered results obtained via the TRELLIS[10] and Step1X-3D[11] methods. We employed Toys4K[15] as our test set.

Baselines. We compare our Texture-VAE at different voxel resolutions with TRELLIS[10]. For the generated results, we also compare with TRELLIS[10], hunyuan3D 2.1[9] and Step1X-3D[11].

Metrics. We use PSNR, LPIPS, and SSIM to evaluate texture reconstruction loss. We use FID[16] and KID[17] to evaluate texture generation quality.

3.2. VAE Reconstruction Evaluation

We conducted a comparative analysis on the reconstruction quality of Texture Variational Autoencoders (VAEs) under different voxel resolutions, with experiments carried out on the original TRELLIS-64, Ours-256, and Ours-512. As shown in tab.1, with the gradual improvement of voxel resolution, the texture reconstruction quality exhibits a significant positive growth trend. Under the 512-resolution condition, the texture reconstruction effect reaches the optimal level.

Combined with the qualitative results in fig.3, we further found that high-resolution voxelization can capture the detailed features of textures more accurately: the texture details are richer and more realistic, and the gap between the reconstructed images and the original ones is significantly reduced. This result strongly demonstrates the key role of high-resolution voxels in improving the quality of texture reconstruction.

3.3. Image to 3D Generation

We have also verified the effectiveness of the Texture-VAE as a foundation model for generation tasks. Tab.2 confirms the validity of our generated results, while the fig.4 presents the visualization results of 3D generation by different

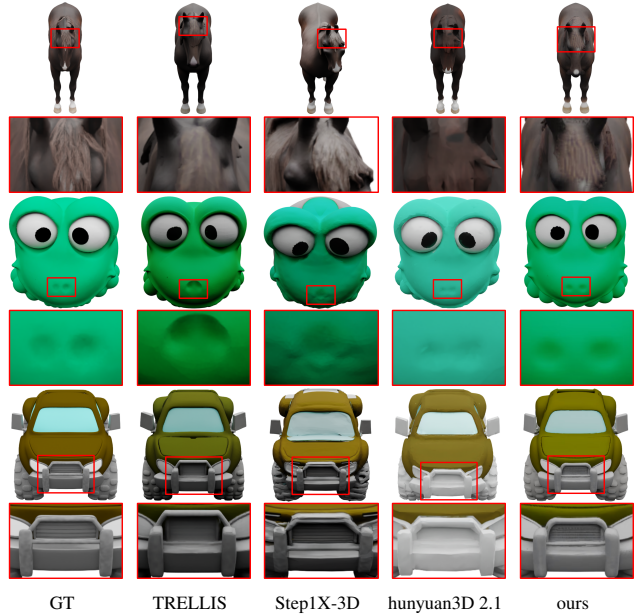


Fig. 4: Qualitative comparison of image to 3D generation.

models. The results show that the generated textures preserve fine details and are highly consistent with the ground-truth images, demonstrating the generality of our method.

3.4. Ablation Studies

We conducted a detailed evaluation of the GPU memory consumption of the generated mask (with redundant points removed during upsampling) and the view-domain partitioning training under different resolutions on an 80GB H100. The relevant results are presented in Table 3. Experimental results show that both the redundant-free upsampling strategy and the view-domain partitioning strategy can significantly reduce GPU memory consumption during the training process, highlighting the efficiency and advantages of our proposed strategies in handling high-resolution data.

Table 3: Comparison of GPU VRAM usage. Unit: MB.

	res-256	res-512
raw	73011	OOM
mask	41577	65537
mask + block 2×2	27881	45811
mask + block 4×4	24541	38301

4. CONCLUSIONS

We have surmounted the constraints of voxel resolution and accomplished high-fidelity texture modeling. Going forward, we will continue to pursue exploration into geometric reconstruction at high resolutions, refine the geometric performance of generated 3D models, and further enhance our framework.

5. REFERENCES

[1] Josh Achiam, Steven Adler, Sandhini Agarwal, Lama Ahmad, Ilge Akkaya, Florencia Leoni Aleman, Diogo Almeida, Janko Altenschmidt, Sam Altman, Shyamal Anadkat, et al., “Gpt-4 technical report,” *arXiv preprint arXiv:2303.08774*, 2023.

[2] Hugo Touvron, Thibaut Lavril, Gautier Izacard, Xavier Martinet, Marie-Anne Lachaux, Timothée Lacroix, Baptiste Rozière, Naman Goyal, Eric Hambro, Faisal Azhar, et al., “Llama: Open and efficient foundation language models,” *arXiv preprint arXiv:2302.13971*, 2023.

[3] Robin Rombach, Andreas Blattmann, Dominik Lorenz, Patrick Esser, and Björn Ommer, “High-resolution image synthesis with latent diffusion models,” in *Proceedings of the IEEE/CVF conference on computer vision and pattern recognition*, 2022, pp. 10684–10695.

[4] Jonathan Ho, Ajay Jain, and Pieter Abbeel, “Denoising diffusion probabilistic models,” *Advances in neural information processing systems*, vol. 33, pp. 6840–6851, 2020.

[5] Team Wan, Ang Wang, Baole Ai, Bin Wen, Chaojie Mao, Chen-Wei Xie, Di Chen, Feiwu Yu, Haiming Zhao, Jianxiao Yang, et al., “Wan: Open and advanced large-scale video generative models,” *arXiv preprint arXiv:2503.20314*, 2025.

[6] Weijie Kong, Qi Tian, Zijian Zhang, Rox Min, Zuozhuo Dai, Jin Zhou, Jiangfeng Xiong, Xin Li, Bo Wu, Jianwei Zhang, et al., “Hunyuanvideo: A systematic framework for large video generative models,” *arXiv preprint arXiv:2412.03603*, 2024.

[7] Bernhard Kerbl, Georgios Kopanas, Thomas Leimkühler, and George Drettakis, “3d gaussian splatting for real-time radiance field rendering.,” *ACM Trans. Graph.*, vol. 42, no. 4, pp. 139–1, 2023.

[8] Longwen Zhang, Ziyu Wang, Qixuan Zhang, Qiwei Qiu, Anqi Pang, Haoran Jiang, Wei Yang, Lan Xu, and Jingyi Yu, “Clay: A controllable large-scale generative model for creating high-quality 3d assets,” *ACM Transactions on Graphics (TOG)*, vol. 43, no. 4, pp. 1–20, 2024.

[9] Team Hunyuan3D, Shuhui Yang, Mingxin Yang, Yifei Feng, Xin Huang, Sheng Zhang, Zebin He, Di Luo, Haolin Liu, Yunfei Zhao, et al., “Hunyuan3d 2.1: From images to high-fidelity 3d assets with production-ready pbr material,” *arXiv preprint arXiv:2506.15442*, 2025.

[10] Jianfeng Xiang, Zelong Lv, Sicheng Xu, Yu Deng, Ruicheng Wang, Bowen Zhang, Dong Chen, Xin Tong, and Jiaolong Yang, “Structured 3d latents for scalable and versatile 3d generation,” in *Proceedings of the Computer Vision and Pattern Recognition Conference*, 2025, pp. 21469–21480.

[11] Weiyu Li, Xuanyang Zhang, Zheng Sun, Di Qi, Hao Li, Wei Cheng, Weiwei Cai, Shihao Wu, Jiarui Liu, Zihao Wang, et al., “Step1x-3d: Towards high-fidelity and controllable generation of textured 3d assets,” *arXiv preprint arXiv:2505.07747*, 2025.

[12] Matt Deitke, Ruoshi Liu, Matthew Wallingford, Huong Ngo, Oscar Michel, Aditya Kusupati, Alan Fan, Christian Laforte, Vikram Voleti, Samir Yitzhak Gadre, et al., “Objaverse-xl: A universe of 10m+ 3d objects,” *Advances in Neural Information Processing Systems*, vol. 36, pp. 35799–35813, 2023.

[13] Jasmine Collins, Shubham Goel, Kenan Deng, Achleshwar Luthra, Leon Xu, Erhan Gundogdu, Xi Zhang, Tomas F Yago Vicente, Thomas Dideriksen, Himanshu Arora, et al., “Abo: Dataset and benchmarks for real-world 3d object understanding,” in *Proceedings of the IEEE/CVF conference on computer vision and pattern recognition*, 2022, pp. 21126–21136.

[14] Huan Fu, Rongfei Jia, Lin Gao, Mingming Gong, Bin-qiang Zhao, Steve Maybank, and Dacheng Tao, “3d-future: 3d furniture shape with texture,” *International Journal of Computer Vision*, vol. 129, no. 12, pp. 3313–3337, 2021.

[15] Stefan Stojanov, Anh Thai, and James M Rehg, “Using shape to categorize: Low-shot learning with an explicit shape bias,” in *Proceedings of the IEEE/CVF conference on computer vision and pattern recognition*, 2021, pp. 1798–1808.

[16] Gaurav Parmar, Richard Zhang, and Jun-Yan Zhu, “On aliased resizing and surprising subtleties in gan evaluation,” in *Proceedings of the IEEE/CVF conference on computer vision and pattern recognition*, 2022, pp. 11410–11420.

[17] Mikołaj Bińkowski, Danica J Sutherland, Michael Arbel, and Arthur Gretton, “Demystifying mmd gans,” *arXiv preprint arXiv:1801.01401*, 2018.